Available online at www.sciencedirect.com
ScienceDirect
Journal of Solid State Chemistry 180 (2007) 349–359
JOURNAL OF SOLID STATE CHEMISTRY
www.elsevier.com/locate/jssc

# *Ln*SrScO4 (*Ln* = La, Ce, Pr, Nd and Sm) systems and structure correlations for $A_2BO_4$ ($K_2NiF_4$) structure types

Rina Patel, Charles Simon, Mark T. Weller*

*School of Chemistry, University of Southampton, University Road, Highfield, Southampton SO17 1BJ, UK*

Received 5 September 2006; received in revised form 13 October 2006; accepted 25 October 2006
Available online 1 November 2006

**Abstract**

The compounds $LnSrScO_4$, where *Ln* = La, Ce, Pr, Nd and Sm, have been synthesized. Rietveld profile analysis of powder X-ray diffraction data collected at room temperature reveal that the compounds possess a modified $K_2NiF_4$-type structure with orthorhombic cell symmetry formed by tilting of the $ScO_6$ octahedra. Variable temperature (25–1200 °C) powder X-ray diffraction data show that at the highest temperatures the structures of $LaSrScO_4$ and $PrSrScO_4$ transform to the regular tetragonal $K_2NiF_4$-structure type but the degree of orthorhombicity ($c/a$) in the unit cells initially increases on heating for all materials, reaching a maximum near 300 °C. This structural behavior is analyzed in terms of relative ionic radii of the various lanthanides and scandium. A general structural model based on tolerance factors has been developed for the family of materials $A_2BO_4$ with various *A* and *B* cation sizes.


*Keywords:* Scandium; $K_2NiF_4$-type structure; Phase transition

## 1. Introduction

The phase behaviors of the ternary $A_2BO_4$ oxides with the $K_2NiF_4$-type [1] structure have received considerable interest in recent years, particularly since the discovery of superconductivity in $La_{2-x}Ba_xCuO_4$ and $Sr_2RuO_4$ [2–4] The idealized, two-dimensional structure of $A_2BO_4$ oxides, $K_2NiF_4$-type, consists of perovskite-like, corner linked $BO_6$ sheets interleaved by rock-salt like *A*O layers. The large *A* cations are arranged in layers with nine nearest O neighbors, 4+4 from one $BO_4$ layer and 1 much shorter interaction from the adjacent layer of stoichiometry $BO_4$, Fig. 1. The $BO_6$ octahedra are not perfectly regular consisting, typically, of four short in-plane *B*–O distances (equatorial) plus two slightly longer apical *B*–O interactions.

As with many complex oxide structures built from $BO_n$ polyhedra the potential exists for these units to tilt or rotate around their centers while maintaining the basic structure type. This has been well studied for perovskite $ABO_3$ structures [5–7] and to a much more limited extent for the double layer Ruddlesden–Popper phases ($A_3B_2O_7$) [8]. Such rotations and tilts of the $BO_n$ polyhedra in these structures generally result in a reduction of the unit cell symmetry but also allows improved coordination to the *A*-type cations. Thus one important factor that determines the structure of the $A_2BO_4$ compounds is the matching between the perovskite-like $BO_6$ layers and the *A*-type cations. A measure of the bond length matching can be calculated from a version of the Goldsmidt tolerance factor $t = (r_A + r_O)/\sqrt{2}(r_B + r_O)$ for perovskite and perovskite-derived structure types; ideal matching between the *A* cation and one layer of linked $BO_6$ octahedra occurs for $t \approx 1$ and the structure formed is tetragonal described in the space group *I*4/*mmm* (no. 139). Ganguly and Rao [9] proposed that $A_2BO_4$ compounds with the *t*-value near the lower limit $t \approx 0.85$ exhibit superlattice reflection lines in their diffraction patterns associated with a rotation of $BO_6$ octahedra around the *c*-axis or a tilting of $BO_6$ octahedra in the 1 0 0 or 1 1 0 direction. This results in orthorhombic deformation of the tetragonal archetype. In these cases two types of orthorhombic distortion have been observed; one is due to the tilting of the $BO_6$ octahedra resulting in the *Abma* space group, as exemplified by $La_2CoO_4$, and the

*Corresponding author.
*E-mail address:* mtw@soton.ac.uk (M.T. Weller).

0022-4596/$ - see front matter © 2006 Elsevier Inc. All rights reserved.
doi:10.1016/j.jssc.2006.10.023

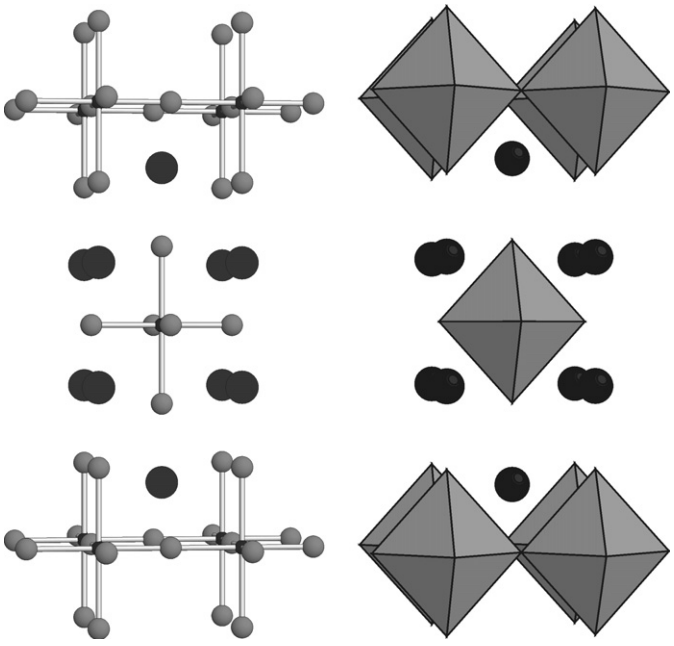

Fig. 1. The ideal $K_2NiF_4$ structure showing the $NiF_6$ octahedra and potassium ions (black spheres).

other can be considered as a consequence of different relative displacements in the positions of the rare earth cations and the oxygen anions generating a structure that can be described in the space group *Fmm*2—as for $Sm_2CoO_4$ [10].

The description of all the possible space groups that may occur for $A_2BO_4$ phases as a result of various octahedral tilts and rotations have been discussed by Hatch et al. [11] In general, however, relatively few materials adopting, or potentially adopting, the $K_2NiF_4$ structure type have been studied in detail structurally. Indeed many compositions have not been previously synthesized and others assumed to adopt the perfect tetragonal structure on the basis of poor quality diffraction data. Furthermore, in most cases only the room temperature structures have been investigated.

Of the few previously studied $A_2BO_4$ complex oxides those adopting the lower symmetry orthorhombic $K_2NiF_4$-type structure, as a result of octahedral tilts or rotations, include the oxygen deficient $La_{1-x}Sr_{1+x}InO_{4-d}$ ($x = 0-0.2$) [12] compounds and $LaSrScO_4$ [13]. $La_{0.8}Sr_{1.2}InO_{3.9}$ crystallizes in the space group *Pbca* (No. 61) and has a calculated *t*-value of 0.9, which suggests that the ionic radius of $In^{3+}$ is too large to form a regular square-net, perovskite-type layer in association with these *A* site cations ($La^{3+}_{0.8}Sr^{2+}_{1.2}$). This results in the formation of a perovskite layer that consists of tilted $InO_{6-y}$ octahedra. $LaSrScO_4$ has been studied using both powder X-ray diffraction (PXD) and dielectric measurements by Kim et al. [13]. This work targeted $Sc^{3+}$ as the *B* site ion of $A_2BO_4$ because $Sc^{3+}$ has the greatest ionic radius among the trivalent 3*d*-transition metal ions and, therefore, was predicted to have the greatest mismatch between the *A* and *B* sites. Rietveld profile refinements carried out using the PXD data investigated three different space groups; *I*4/*mmm*, *Fmmm* and *Abma*. On the basis of the lower profile fit *R* factors obtained for the refinements with the space groups *Fmmm* and *Abma* it was concluded that these two space groups offered the best descriptions of the structure adopted by $LaSrScO_4$. *Abma*, which can involve a tilting of the $ScO_6$ octahedra, was chosen as the most plausible based on the dielectric measurements.

In this work we have studied the effect on the $K_2NiF_4$ structure type of introducing an even greater mismatch in the *A* and *B* ion sizes caused by reducing the effective ionic radius of the *A* site in the series of compounds $LnSrScO_4$ ($Ln$ = La, Ce, Pr, Nd and Sm). We have also investigated the effect of temperature on the structures and phases behaviors of these materials. Using this information the relationship between *A* and *B* cation sizes and choice of structure in the general $A_2BO_4$ system is discussed.

## 2. Experimental

$LnSrScO_4$ ($Ln$ = La, Pr, Nd and Sm) phases were synthesized by the direct reaction of stoichiometric amounts of $Ln_2O_3$ (99.99%, Aldrich) ($Ln$ = La, Nd and Sm), $Pr_6O_{11}$ (99.99%, Aldrich), $SrCO_3$ (99.9+%, Aldrich) and $Sc_2O_3$ (99.9%, Avocado). The lanthanide oxides were dried in air at 800 °C for 24 h prior to use. The starting materials were intimately ground as a suspension in ethanol, which was subsequently evaporated. The mixed powders were pressed into pellets of 10 mm diameter and 3 mm thickness under 10 tonnes of pressure and these were then fired at 1200 °C for 48 h. Samples were cooled, ground, reformed into pellets and heated again in air at 1350 °C for 48 h and the products quenched to room temperature to obtain a near single phase product; very weak peaks ($I/I_0$~0.01) in the powder diffraction patterns of some products could be assigned to unreacted $Ln_2O_3$. Attempts to prepare $LaBaScO_4$ using the same procedure results in the part formation of the required phase but in combination with the double layered Ruddlesden–Popper phase $La_2BaSc_2O_7$. $CeSrScO_4$ was synthesized via a sol–gel route, whereby stoichiometric amounts of $Ce(NO_3)_3 \cdot 6H_2O$, $Sr(NO_3)_2$ and $Sc_2O_3$ were dissolved in the minimum quantity of 15.8 M nitric acid. Molar equivalents of ethylene glycol and citric acid dissolved in ~25 mL distilled water was added to this solution. The mixture was heated to 400 °C in air for 48 h and then 1200 °C under $H_2/N_2$ for a further 48 h. Following regrinding and pelletization the sample was annealed under 5% $H_2/N_2$ for another 48 h at 1350 °C; these conditions avoid the potential for oxidation of Ce(III) to Ce(IV). Attempts to prepare $LnSrScO_4$ phases under similar conditions with the other heavier, smaller ionic radius lanthanide trivalent cations, Eu–Lu, were unsuccessful.

$LnSrScO_4$ ($Ln$ = La, Ce, Pr, Nd and Sm) samples were characterized using powder X-ray diffraction (PXD). PXD data were initially collected at room temperature over the

$2\theta$ range 10–100° using a Siemens D5000 diffractometer operating with $Cu_{K\alpha 1}$ radiation. Variable temperature PXD data were collected over the $2\theta$ range 10–100° using a step size of 0.018° using a Bruker D8 diffractometer in conjunction with a position sensitive detector and an Anton–Paar HTK 1200 furnace stage.

## 3. Results

In order to determine the correct structural description for the $Ln$SrScO$_4$ compounds, initial detailed analysis centered on the room temperature data from LaSrScO$_4$. Rietveld refinements [14,15] using the GSAS [16] suite of programmes and PXD data obtained for LaSrScO$_4$ were performed in the different space groups accommodating various octahedral tilts as proposed by Hatch et al. [11]. For each structural description the appropriate model was set-up within GSAS and identical numbers of profile parameters refined; the number of atomic positional parameters, which varied as a function of the structural model, is included in Table 1. Table 1 also summarizes the degree of success achieved in fitting each of these structural models to the data obtained. Two crystallographic descriptions clearly model the data better than the others, *Abma* and *Pccn*. Of these the higher symmetry *Abma* was chosen as it is a simpler model, requires three less positional parameters to describe the structure and no diffraction intensity was observed at the calculated reflection positions that were allowed and unique to the *Pccn* description (corresponding to $h\,k\,l$ with $k+l = 2n+1$, e.g. 1 1 0, 1 1 2, 1 1 4). In the *Abma* description, also used by Kim et al. [13], the lanthanum and strontium are fully disordered and situated on ($x$,0,$z$), $x\sim0.02$, $z\sim0.36$; scandium on (0,0,0) and oxygen atoms on (0.25,0.25,$z$) $z\sim0.02$ and on ($x$,0,$z$) $x\sim0.45$, $z\sim0.33$. As with the *I4/mmm* crystal structure description for $K_2NiF_4$ phases, the *B*-type/$Sc^{3+}$ ions occupy sites with a distorted octahedral coordination to oxygen and the $Sr^{2+}$ and $Ln^{3+}$ ions occupy sites having a coordination number of 9, though variation in bond lengths to oxygen are much larger than for the regular tetragonal $K_2NiF_4$ structure. Final stages of the refinements of the structure in the *Abma* description included all global parameters, i.e. histogram scale factor, peak shape, zero point displacement, background parameters and lattice constants; all isotropic temperature factors and atom positions were varied and unconstrained. The data in Table 2 summarize this crystallographic model, the fit to the profile acheived and provides a comparision with the model published by Kim et al. [13]. Fig. 2 shows the results of the structural refinement in terms of the profile fit achieved for the data collected from LaSrScO$_4$ at room temperature.

Table 1
Refined lattice parameters and final fit parameters for room temperature LaSrScO$_4$ PXD data in space groups accommodating different octahedral tilts

| Space group | Latice parameters | | | $\chi^2$ | $R_{wp}$ (%) | $R_p$(%) | No. of atomic positional parameters varied |
|---|---|---|---|---|---|---|---|
| | *a* | *b* | *c* | | | | |
| *I4/mmm* | 4.06993(8) | 4.06993(8) | 12.46755(32) | 4.354 | 5.12 | 3.73 | 2 |
| *Abma* | 5.76147(14) | 5.74991(14) | 12.46744(23) | 2.898 | 4.17 | 3.11 | 5 |
| *Pbca* | 12.4674(4) | 5.76192(26) | 5.74985(27) | 9.959 | 7.73 | 4.94 | 9 |
| *Pccn* | 5.76159(13) | 5.74965(13) | 12.46759(23) | 2.863 | 4.14 | 3.09 | 8 |
| *Fmmm* | 5.76185(14) | 5.74932(14) | 12.46742(25) | 3.714 | 4.72 | 3.45 | 2 |

Table 2
Refined atomic positions for LaSrScO$_4$ at room temperature

| Atom | *x* | *y* | *z* | Occupancy | $U_{iso} \times 100$ (Å$^2$) |
|---|---|---|---|---|---|
| La | 0.01368(30)<br>*0.0146(9)* | 0 | 0.35653(6)<br>*0.3566(3)* | 0.5 | 1.36(5)<br>*0.68* |
| Sr | 0.01368(30)<br>*0.0146(9)* | 0 | 0.35653(6)<br>*0.3566(3)* | 0.5 | 1.36(5)<br>*0.68* |
| Sc | 0 | 0 | 0 | 1 | 0.42(8)<br>*0.50* |
| O1 | 0.25 | 0.25 | 0.0154(9)<br>*0.0137(6)* | 1 | 1.97(21)<br>*2.54* |
| O2 | 0.4353(16)<br>*0.4514(85)* | 0 | 0.4353(16)<br>*0.3297(28)* | 1 | 1.97(21)<br>*2.90* |

Space group *Abma*; $a = 5.76147(14)$, *5.7657(5)*; $b = 5.74991(14)$, *5.7513(4)*; $c = 12.46744(23)$, *12.467(1)* Å (estimated standard deviations in parentheses; parameters from Kim et al. [13] are given in italics).
$R_p = 3.11\%$, $R_{wp}$ 4.17% = , $\chi^2 = 2.898$.

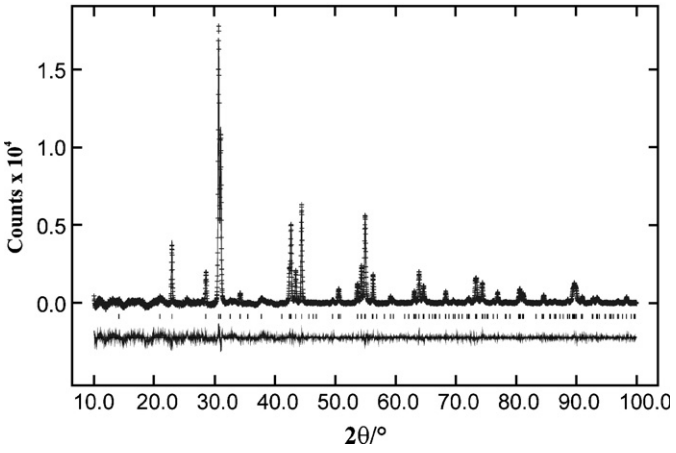


Fig. 2. Powder X-ray diffraction data profile fit for orthorhombic $LaSrScO_4$ at room temperature. (Crosses indicate observed data, the upper continuous line shows the calculated profile, the lower continuous line the difference. Tick marks show reflection positions.)

The room temperature model was subsequently used to successfully fit the diffraction data obtained from $LaSrScO_4$ at temperatures between 25 and 800 °C, though above 500 °C the orthorhombicity in the unit cell decreased significantly. Data collected above 800 °C could be fully modeled in the tetragonal space group *I4/mmm* (i.e. a regular tetragonal $K_2NiF_4$ type structure) with similar fit factors to the orthorhombic *Abma* and therefore refinements were undertaken using this simpler crytallographic description.

For the other scandate phases, $LnSrScO_4$ ($Ln$ = Ce, Pr, Nd and Sm), a similar analysis was undertaken. Initial modeling of the data collected at room temperature for each different lanthanide phase confirmed that the appropriate choice of space group was the orthorhombic *Abma,* while at high temperatures the diffraction data from the $PrSrScO_4$ phase could again be modeled in the simpler tetragonal *I4/mmm* description. For all lanthanides and all temperatures for which data were collected, structure refinements were completed to convergence to include all profile and positional parameters. No evidence for the displacement of the scandium ion from the center of the $ScO_6$ octahedron was found with reasonable, low thermal displacement parameters determined for this site. The unit cells of the *I4/mmm* ($a_T \times a_T \times c_T$) and *Abma* descriptions are related via the relationship $\sqrt{2}a_T \times \sqrt{2}a_T \times c_T$, allowing direct comparison of the values extracted from the refinements. The refined structural parameters for all phases as a function of temperature are summarized in Table 3. Table 4 details the extracted important interatomic distances and bond angles of these compounds as a function of temperature. Variable temperature PXD data for $CeSrScO_4$ were collected under a constant flow of nitrogen with the aim of preventing oxidation of Ce(III) to Ce(IV), however from detailed analysis of the thermodiffractogram and Rietveld refinements using the high temperature data it was clear that above 400 °C the compound started to oxidize. This resulted in the formation of an impurity with a cubic structure (of possible stoichiometry of $(Sr^{2+}Ce^{3+})(Ce^{4+}Sc^{3+})O_3$) and data collected above 500 °C from this phase was not analyzed further. Data sets collected at 400 and 500 °C were analyzed using GSAS as the only observable phase in the diffraction patterns was $CeSrScO_4$, but the results obtained are treated separately due to the possible structural influences of the onset of decomposition.

The orthorhombic nature of the crystal distortion in the scandium compounds at room temperature results from the tilting of the $ScO_6$ octahedra within the perovskite layer. Analyses of the variable temperature data allowed elucidation of this structural distortion as a function of temperature for these compounds. Graphs of the *a* and *b* lattice parameters (converted to a pseudo-orthorhombic description for the highest temperatures) as a function of temperature for $LaSrScO_4$ (Fig. 3) and temperature against *a*/*b* ratio for $LnSrScO_4$ ($Ln$ = La, Ce, Pr, Nd and Sm) (Fig. 4) have been plotted. It can be seen that in all compounds the level of distortion increases in the temperature range 25–300 °C and then decreases in the temperature range 300–1200 °C; for $LaSrScO_4$ and $PrSrScO_4$ the compounds convert to the ideal $K_2NiF_4$ type structure at approximately 900 and 1000 °C, respectively.

Octahedral tilting in the *Abma* space group causes the coordination sphere about the $Ln^{3+}$ cation to change dramatically, in comparison with the $Ln^{3+}$ coordination sphere in the *I4/mmm* space group, while the coordination geometry around the $Sc^{3+}$ ion is left virtually unchanged. Therefore, it is logical to assume that the octahedral tilting is driven by the need to optimize the anion coordination about the *A* site (particularly the $Ln^{3+}$ cation) resulting in the most energetically favorable configuration and distances. This optimization is more difficult to achieve in *I4/mmm* with the forced 1+4+4 coordination for the *A* site. The Sc–O–Sc bond angles, which connect the $ScO_6$ octahedra, provide a measure of the degree of tilting of the octahedra and were determined as 169.1(6)°, 170.6(10)°, 166.0(8)°, 167.3(9)° and 162.8(9)° for $LaSrScO_4$, $CeSrScO_4$, $PrSrScO_4$, $NdSrScO_4$ and $SmSrScO_4$, respectively, at room temperature. While the correlation is not perfect, it demonstrates a clear trend towards an increased tilt of the octahedra as the average ionic radius of the *A* site cations decreases. In tetragonal $K_2NiF_4$-type $A_2BO_4$ oxide, $BO_6$ octahedra of the perovskite layer connect with each other at an angle of 180°.

Figs. 5 and 6 show the coordination environment of $Sc^{3+}$ and $La^{3+}/Sr^{2+}$ sites at room temperature (*Abma*) and $La^{3+}/Sr^{2+}$ (*I4/mmm*) at 1000 °C in $LaSrScO_4$. The effect of the tilting of the octahedra at 25 °C can be clearly seen and the effect is most apparent in the coordination environment of the *A* site cations. The $K_2NiF_4$ structure adopted at the highest temperature produces the more regular 1+4+4 environment for (La,Sr) site with one very short contact ( 2.35 Å) and 8 further contacts in the range 2.7–3.0 Å. The effect of the octahedral titling at room

Table 3
Extracted positional parameters using the *Abma* model in Table 2 and *I4/mmm* for $LnSrScO_4$ as a function of temperature

| Temperature (°C) | *a* (Å) | *b* (Å) | *c* (Å) | *Ln*/Sr(*x*) | *Ln*/Sr(*z*) | O1(*z*) | O2(*x*) | O2(*z*) | *Ln*/Sr Ui/Ue × 100 Å$^2$ | Sc Ui/Ue × 100 Å$^2$ | O1/O2 Ui/Ue × 100 Å$^2$ |
|---|---|---|---|---|---|---|---|---|---|---|---|
| *$LaSrScO_4$* | | | | | | | | | | | |
| 25 | 5.76147(14) | 5.74991(14) | 12.46744(23) | 0.01368(30) | 0.35653(6) | 0.0154(9) | 0.4353(16) | 0.3307(6) | 1.36(5) | 0.42(8) | 1.97(21) |
| 50 | 5.76125(14 | 5.74942(14) | 12.47334(24) | 0.01334(31) | 0.35653(6) | 0.0146(10) | 0.4356(16) | 0.3309(6) | 1.62(5) | 0.54(8) | 2.14(21) |
| 100 | 5.76251(13) | 5.74985(14) | 12.48833(23) | 0.01293(32) | 0.35652(6) | 0.0158(9) | 0.4357(16) | 0.3310(6) | 1.70(5) | 1.19(8) | 2.18(21) |
| 200 | 5.76715(13) | 5.74905(13) | 12.52060(25) | 0.0114(4) | 0.35631(7) | 0.0148(11) | 0.4437(18) | 0.3317(6) | 2.09(5) | 0.82(9) | 2.77(22) |
| 300 | 5.77358(13) | 5.74816(13) | 12.55409(28) | 0.0098(5) | 0.35616(7) | 0.0121(13) | 0.4508(21) | 0.3308(6) | 2.39(6) | 1.11(10) | 3.58(23) |
| 400 | 5.77598(13) | 5.75102(13) | 12.58484(27) | 0.0090(5) | 0.35600(7) | 0.0093(16) | 0.4529(22) | 0.3310(6) | 2.67(4) | 1.42(9) | 4.12(22) |
| 500 | 5.77772(12) | 5.75570(12) | 12.61196(26) | 0.0085(5) | 0.35589(7) | 0.0050(20) | 0.4538(22) | 0.3307(6) | 2.93(4) | 1.63(9) | 4.38(21) |
| 600 | 5.78013(12) | 5.75950(12) | 12.64099(24) | 0.0063(6) | 0.35586(6) | −0.0130(12) | 0.4500(20) | 0.3302(6) | 3.23(4) | 2.43(9) | 4.46(23) |
| 700 | 5.78117(12) | 5.76310(12) | 12.67185(24) | 0.050(6) | 0.35579(7) | −0.0139(12) | 0.4481(19) | 0.3290(5) | 3.39(6) | 2.61(10) | 4.21(24) |
| 800 | 5.78016(13) | 5.76802(13) | 12.70312(23) | 0.0033(6) | 0.35568(7) | −0.0155(11) | 0.4465(19) | 0.3289(5) | 3.58(6) | 2.80(10) | 4.02(24) |
| 900 | 4.08413(6) | 4.08413(6) | 12.73932(23) | | 0.35550(7) | | | 0.1720(6) | 3.67(6) | 2.93(11) | 6.49(18) |
| 1000 | 4.08769(6) | 4.08769(6) | 12.76964(23) | | 0.35555(7) | | | 0.1716(6) | 3.79(6) | 2.93(11) | 6.54(18) |
| *$CeSrScO_4$* | | | | | | | | | | | |
| 25 | 5.76064(19) | 5.74590(20) | 12.3942(4) | 0.0162(4) | 0.35596(11) | 0.0135(15) | 0.4140(22) | 0.3307(11) | 2.65(9) | 2.14(15) | 2.80(32) |
| 50 | 5.76070(19) | 5.74488(20) | 12.3989(4) | 0.0162(4) | 0.35580(11) | 0.0128(15) | 0.4170(22) | 0.3328(11) | 2.28(8) | 1.61(15) | 2.36(32) |
| 100 | 5.76243(19) | 5.74480(19) | 12.4125(4) | 0.0158(4) | 0.35581(11) | 0.0122(16) | 0.4172(22) | 0.3332(11) | 2.75(32) | 1.91(15) | 2.75(32) |
| 200 | 5.76605(19) | 5.74622(20) | 12.4467(4) | 0.0144(5) | 0.35533(11) | 0.0117(17) | 0.4182(23) | 0.3339(11) | 2.96(9) | 2.15(16) | 3.61(34) |
| 300 | 5.77117(18) | 5.74881(19) | 12.4857(4) | 0.0130(5 | 0.35498(11) | 0.0103(18) | 0.4228(22) | 0.3333(10) | 3.17(10) | 2.36(16) | 3.49(33) |
| 400 | 5.76487(30) | 5.75227(33) | 12.5451(5) | 0.0102(8) | 0.35359(14) | 0.0105(21) | 0.4055(24) | 0.3383(13) | 4.16(9) | 2.81(18) | 4.2(4) |
| 500 | 5.77979(26 | 5.76799(28) | 12.5744(5) | 0.0076(8) | 0.35054(15) | 0.076(24) | 0.3929(23) | 0.3388(15) | 4.97(9) | 1.17(16) | 5.7(4) |
| *$PrSrScO_4$* | | | | | | | | | | | |
| 25 | 5.76247(17) | 5.73387(15) | 12.3206(24) | 0.01850(35) | 0.35622(10) | 0.0198(12) | 0.4351(24) | 0.3358(10) | 1.98(8) | 1.11(14) | 3.27(29) |
| 50 | 5.76337(17) | 5.73267(15) | 12.3261(4) | 0.00176(4) | 0.35601(10) | 0.0185(12) | 0.4348(23) | 0.3362(10) | 1.97(8) | 0.93(14) | 2.88(29) |
| 100 | 5.76667(17) | 5.73076(16) | 12.3417(4) | 0.0177(4) | 0.35592(10) | 0.0193(12) | 0.4350(23) | 0.3355(10) | 2.07(8) | 1.10(14) | 3.18(29) |
| 200 | 5.77360(17) | 5.72858(15) | 12.3760(4) | 0.0174(4) | 0.35571(10) | 0.0199(12) | 0.4376(23) | 0.3354(10) | 2.52(9) | 1.53(15) | 3.66(30) |
| 300 | 5.77846(17) | 5.72960(16) | 12.4097(4) | 0.0162(4) | 0.35572(10) | 0.0207(11) | 0.4381(22) | 0.3348(9) | 2.56(9) | 1.48(15) | 2.00(30) |
| 400 | 5.78091(16) | 5.73350(16) | 12.4402(4) | 0.0155(4) | 0.35543(10) | 0.00195(12) | 0.4457(24) | 0.2240(17) | 2.79(10) | 1.69(15) | 3.55(29) |
| 500 | 5.78245(15) | 5.73894(15) | 12.4698(4) | 0.0140(5) | 0.35512(10) | 0.0214(11) | 0.446(23) | 0.3347(9) | 3.10(9) | 2.02(15) | 3.46(29) |
| 600 | 5.78475(14) | 5.74503(15) | 12.4989(4) | 0.0129(5) | 0.35500(10) | 0.0223(10) | 0.4473(24) | 0.3345(8) | 3.35(9) | 2.00(15) | 3.40(29) |
| 700 | 5.78670(15) | 5.75084(16) | 12.5278(4) | 0.0134(5) | 0.35483(10) | 0.0206(12) | 0.4496(25) | 0.3343(8) | 3.69(10) | 2.43(16) | 4.21(30) |
| 800 | 5.78763(15) | 5.75635(15) | 12.5565(4) | 0.0124(6) | 0.35482(11) | 0.0184(13) | 0.4498(27) | 0.3337(9) | 3.71(10) | 2.61(16) | 4.48(32) |
| 900 | 5.78844(20) | 5.76232(20) | 12.5866(5) | 0.0114(7) | 0.35486(12) | 0.0165(17) | 0.4446(31) | 0.3345(10) | 3.93(12) | 2.93(19) | 4.8(4) |
| 1000 | 5.78783(19) | 5.76869(18) | 12.6208(4) | 0.0095(8) | 0.35480(12) | 0.0192(14) | 0.4397(28) | 0.3327(9) | 4.29(8) | 3.36(17) | 4.4(4) |
| 1100 | 4.08744(11) | 4.08744(11) | 12.6570(4) | | 0.35460(13) | | | 0.1700(11) | 4.21(8) | 4.69(19) | 8.25(31) |
| 1200 | 4.08898(10) | 4.08898(10) | 12.6944(4) | | 0.35478(13) | | | 0.1696(11) | 4.09(7) | 4.52(19) | 8.68(33) |

Table 3 (*continued*)

| Temperature (°C) | $a$ (Å) | $b$ (Å) | $c$ (Å) | $Ln$/Sr($x$) | $Ln$/Sr($z$) | O1($z$) | O2($x$) | O2($z$) | $Ln$/Sr Ui/Ue × 100 Å$^2$ | Sc Ui/Ue × 100 Å$^2$ | O1/O2 Ui/Ue × 100 Å$^2$ |
|---|---|---|---|---|---|---|---|---|---|---|---|
| *$NdSrScO_4$* | | | | | | | | | | | |
| 25 | 5.74186(22) | 5.70079(19) | 12.2437(4) | 0.0182(4) | 0.35609(10) | 0.0177(14) | 0.4369(27) | 0.3240(10) | 2.33(5) | 0.91(13) | 3.54(29) |
| 50 | 5.76166(24) | 5.71915(20) | 12.2904(5) | 0.0179(4) | 0.35641(11) | 0.0187(15) | 0.4409(30) | 0.3235(11) | 2.41(6) | 0.99(15) | 3.76(32) |
| 100 | 5.76115(23) | 5.71624(20) | 12.2988(5) | 0.0182(4) | 0.35623(11) | 0.0193(14) | 0.4386(28) | 0.3251(11) | 2.19(6) | 0.96(16) | 3.09(32) |
| 200 | 5.76889(24) | 5.71943(20) | 12.3366(5) | 0.0189(4) | 0.35598(11) | 0.0221(12) | 0.4379(16) | 0.3262(10) | 2.23(7) | 0.87(16) | 2.66(31) |
| 300 | 5.77348(21) | 5.72278(19) | 12.3678(5) | 0.0163(5) | 0.35566(11) | 0.0166(15) | 0.4372(26) | 0.3285(11) | 2.50(7) | 0.79(15) | 3.40(33) |
| 400 | 5.77627(21) | 5.72676(19) | 12.3955(5) | 0.0158(5) | 0.35566(11) | 0.0137(17) | 0.4376(27) | 0.3281(10) | 2.65(7) | 0.98(15) | 4.22(33) |
| 500 | 5.77871(21) | 5.73186(21) | 12.4223(5) | 0.0156(5) | 0.35537(11) | 0.0116(20) | 0.4363(28) | 0.3267(11) | 2.88(7) | 1.32(16) | 4.7(4) |
| 600 | 5.77929(21) | 5.73630(22) | 12.4443(5) | 0.0146(6) | 0.35507(12) | 0.0120(22) | 0.4339(30) | 0.3281(12) | 3.05(8) | 1.35(17) | 4.8(4) |
| 700 | 5.78090(20) | 5.74174(22) | 12.4705(5) | 0.0131(7) | 0.35483(13) | 0.0075(27) | 0.4385(31) | 0.3275(11) | 3.30(8) | 1.39(17) | 4.9(4) |
| 800 | 5.78224(21) | 5.74675(23) | 12.4973(5) | 0.0125(8) | 0.35464(14) | 0.0041(38) | 0.446(4) | 0.3271(12) | 3.66(9) | 1.89(18) | 6.4(4) |
| 900 | 5.78310(24) | 5.75185(25) | 12.5254(6) | 0.0125(9) | 0.35432(15) | 0.0013(35) | 0.450(4) | 0.3278(13) | 3.91(10) | 2.21(20) | 6.7(5) |
| 1000 | 5.78378(25) | 5.75857(25) | 12.5581(6) | 0.0099(11) | 0.35397(15) | −0.0081(35) | 0.445(4) | 0.3271(13) | 4.39(10) | 2.67(21) | 6.3(5) |
| *$SmSrScO_4$* | | | | | | | | | | | |
| 25 | 5.73826(22) | 5.69938(21) | 12.2946(5) | 0.00186(5) | 0.35416(15) | 0.0252(12) | 0.4138(25) | 0.3357(14) | 2.42(8) | 1.78(19) | 2.3(4) |
| 50 | 5.73924(21) | 5.69858(20) | 12.2952(5) | 0.0195(5) | 0.35427(14) | 0.0236(12) | 0.4177(24) | 0.3368(13) | 1.96(8) | 1.02(18) | 1.38(35) |
| 100 | 5.74268(21) | 5.69860(20) | 12.2984(5) | 0.0192(5) | 0.35421(14) | 0.0252(11) | 0.4169(23) | 0.3363(13) | 1.97(8) | 1.05(18) | 1.08(34) |
| 200 | 5.75139(21) | 5.70146(18) | 12.3025(5) | 0.0185(5) | 0.35456(14) | 0.0228(12) | 0.4224(24) | 0.3372(12) | 2.02(18) | 1.29(18) | 1.77(34) |
| 300 | 5.75731(21) | 5.70594(18) | 12.3166(5) | 0.0193(5) | 0.35464(14) | 0.0228(12) | 0.4244(24) | 0.3381(13) | 2.24(8) | 1.84(19) | 2.41(34) |
| 400 | 5.76108(21) | 5.71089(18) | 12.3368(5) | 0.0191(5) | 0.35443(14) | 0.0219(13) | 0.4254(24) | 0.3389(13) | 2.47(8) | 1.95(19) | 2.51(34) |
| 500 | 5.76412(21) | 5.71649(20) | 12.3590(5) | 0.0194(50 | 0.35429(14) | 0.0224(13) | 0.4269(25) | 0.3395(13) | 2.63(9) | 2.24(20) | 2.9(4) |
| 600 | 5.76734(21) | 5.72242(21) | 12.3828(5) | 0.0183(5) | 0.35424(14) | 0.0226(13) | 0.4261(25) | 0.3398(13) | 2.98(9) | 2.79(21) | 3.4(4) |
| 700 | 5.76938(21) | 5.72793(22) | 12.4063(6) | 0.0177(5) | 0.35407(14) | 0.0234(14) | 0.4331(27) | 0.3395(13) | 3.29(9) | 3.02(21) | 4.2(4) |
| 800 | 5.77219(21) | 5.73340(22) | 12.4295(6) | 0.0170(6) | 0.35388(15) | 0.0226(15) | 0.4353(29) | 0.3393(13) | 3.61(10) | 3.39(22) | 5.1(4) |
| 900 | 5.77389(20) | 5.73903(21) | 12.4561(5) | 0.0163(6) | 0.35366(15) | 0.0217(16) | 0.4342(29) | 0.3389(13) | 3.75(10) | 3.59(22) | 5.5(4) |
| 1000 | 5.77630(23) | 5.74567(24) | 12.4856(6) | 0.0144(7) | 0.353332(16) | 0.0227(16) | 0.4348(31) | 0.3387(13) | 4.04(11) | 4.17(24) | 5.3(5) |

Estimated standard deviations in parentheses.

Table 4
Extracted bond distances and angles of interest

| Temperature (°C) | Sc–O(1) (Å) | Sc–O(2) (Å) | Ln/Sr–O(1) × 2 (Å) | Ln/Sr–O(1) × 2 (Å) | Ln/Sr–O(2) (Å) | Ln/Sr–O(2) × 2 (Å) | Ln/Sr–O(2) (Å) | Ln/Sr–O(2) (Å) | Sc–O(1)–Sc (°) |
|---|---|---|---|---|---|---|---|---|---|
| *$LaSrScO_4$* | | | | | | | | | |
| 25 | 2.145(7) | 2.0441(10) | 2.801(8) | 2.630(7) | 2.445(9) | 2.9087(13) | 2.378(7) | 3.353(9) | 169.1(6) |
| 50 | 2.141(7) | 2.0430(11) | 2.795(9) | 2.636(8) | 2.449(9) | 2.9131(13) | 2.381(8) | 3.344(9) | 169.8(7) |
| 100 | 2.143(7) | 2.0447(11) | 2.809(8) | 2.627(7) | 2.452(9) | 2.9138(13) | 2.384(7) | 3.332(9) | 168.9(6) |
| 200 | 2.131(8) | 2.0442(12) | 2.810(10) | 2.635(8) | 2.504(10) | 2.9114(13) | 2.386(8) | 3.284(10) | 169.6(7) |
| 300 | 2.143(8) | 2.0424(12) | 2.796(12) | 2.655(11) | 2.555(11) | 2.9131(13) | 2.371(8) | 3.235(11) | 171.5(9) |
| 400 | 2.144(8) | 2.0411(11) | 2.780(14) | 2.679(13) | 2.572(12) | 2.9133(13) | 2.376(8) | 3.220(11) | 173.4(11) |
| 500 | 2.152(7) | 2.0398(8) | 2.716(170 | 2.749(18) | 2.583(12) | 2.9144(13) | 2.374(8) | 3.216(11) | 176.1(14) |
| 600 | 2.166(7) | 2.0466(13) | 2.608(10) | 2.866(10) | 2.576(11) | 2.9191(11) | 2.374(7) | 3.220(11) | 170.7(9) |
| 700 | 2.187(7) | 2.0483(13) | 2.610(9) | 2.874(10) | 2.576(11) | 2.9229(14) | 2.365(7) | 3.227(10) | 170.1(8) |
| 800 | 2.195(7) | 2.0510(13) | 2.605(8) | 2.889(9) | 2.578(11) | 2.9244(14) | 2.368(7) | 3.230(11) | 168.9(8) |
| | | | Ln/Sr–O(1) × 4/Å | | Ln/Sr–O(2)/Å | Ln/Sr–O(2) × 4/Å | | | Sc–O(1)–Sc/° |
| 900 | 2.192(7) | 2.04206(3) | 2.7493(6) | | 2.337(8) | 2.9091(9) | | | 180 |
| 1000 | 2.191(8) | 2.04385(3) | 2.7531(6) | | 2.350(8) | 2.9111(9) | | | 180 |
| *$CeSrScO_4$* | | | | | | | | | |
| 25 | 2.156(13) | 2.0410(15) | 2.773(13) | 2.652(11) | 2.312(13) | 2.9178(23) | 2.387(13) | 3.486(13) | 170.6(10) |
| 50 | 2.128(13) | 2.0401(14) | 2.768(13) | 2.659(12) | 2.326(13) | 2.9122(22) | 2.407(13) | 3.462(13) | 171.1(10) |
| 100 | 2.124(13) | 2.0399(15) | 2.767(14) | 2.663(12) | 2.330(13) | 2.9118(22) | 2.414(13) | 3.459(13) | 171.5(11) |
| 200 | 2.121(13) | 2.0403(15) | 2.774(15) | 2.670(13) | 2.343(13) | 2.9115(22) | 2.420(14) | 3.448(13) | 171.8(12) |
| 300 | 2.129(13) | 2.0405(14) | 2.774(16) | 2.683(14) | 2.381(13) | 2.9108(21) | 2.408(13) | 3.417(13) | 172.8(13) |
| 400 | 2.100(16) | 2.0402(17) | 2.802(19) | 2.688(17) | 2.287(14) | 2.9231(28) | 2.482(16) | 3.491(14) | 172.6(15) |
| 500 | 2.120(18) | 2.0436(14) | 2.818(22) | 2.735(20) | 2.232(14) | 2.9445(30) | 2.471(19) | 3.556(14) | 174.6(17) |
| *$PrSrScO_4$* | | | | | | | | | |
| 25 | 2.058(13) | 2.0469(17) | 2.813(10) | 2.600(8) | 2.409(13) | 2.8919(17) | 2.408(13) | 3.378(13) | 166.0(8) |
| 50 | 2.054(12) | 2.0450(16) | 2.803(10) | 2.613(9) | 2.417(13) | 2.8898(16) | 2.417(12) | 3.376(18) | 167.2(8) |
| 100 | 2.065(12) | 2.0464(17) | 2.813(10) | 2.609(9) | 2.419(13) | 2.8894(17) | 2.410(12) | 3.378(13) | 166.6(8) |
| 200 | 2.069(12) | 2.0482(17) | 2.825(10) | 2.609(9) | 2.439(13) | 2.8870(16) | 2.439(13) | 3.364(13) | 166.2(8) |
| 300 | 2.081(12) | 2.0505(17) | 2.840(10) | 2.602(8) | 2.452(13) | 2.8887(16) | 2.407(12) | 3.353(13) | 165.6(8) |
| 400 | 2.089(11) | 2.0499(17) | 2.838(11) | 2.614(9) | 2.501(13) | 2.8879(15) | 2.391(11) | 3.307(13) | 166.4(8) |
| 500 | 2.086(11) | 2.0542(18) | 2.868(10) | 2.600(8) | 2.503(13) | 2.8907(15) | 2.400(11) | 3.307(13) | 165.0(7) |
| 600 | 2.0572(18) | 2.090(10) | 2.884(10) | 2.594(8) | 2.526(13) | 2.8930(14) | 2.399(11) | 3.295(13) | 164.4(7) |
| 700 | 2.0558(18) | 2.096(11) | 2.873(11) | 2.613(9) | 2.537(14) | 2.8949(15) | 2.398(11) | 3.270(14) | 165.6(8) |
| 800 | 2.108(11) | 2.0538(19) | 2.860(12) | 2.629(10) | 2.545(15) | 2.8986(16) | 2.395(11) | 3.272(15) | 167.1(9) |
| 900 | 2.0527(21) | 2.114(12) | 2.852(15) | 2.640(13) | 2.516(16) | 2.9050(20) | 2.411(13) | 3.297(16) | 168.2(11) |
| 1000 | 2.0577(21) | 2.145(12) | 2.888(14) | 2.616(12) | 2.499(15) | 2.9142(21) | 2.399(12) | 3.317(15) | 166.2(10) |
| | | | Ln/Sr–O(1) × 4/Å | | Ln/Sr–O(2)/Å | Ln/Sr–O(2) × 4/Å | | | Sc–O(1)–Sc/° |

Table 4 (*continued*)

| Temperature (°C) | Sc–O(1) (Å) | Sc–O(2) (Å) | Ln/Sr–O(1) × 2 (Å) | Ln/Sr–O(1) × 2 (Å) | Ln/Sr–O(2) (Å) | Ln/Sr–O(2) × 2 (Å) | Ln/Sr–O(2) (Å) | Ln/Sr–O(2) (Å) | Sc–O(1)–Sc (°) |
|---|---|---|---|---|---|---|---|---|---|
| 1100 | 2.04372(5) | 2.151(14) | 2.7502(11) | | 2.337(14) | 2.9069(15) | | | 180 |
| 1200 | 2.04449(5) | 2.153(14) | 2.7528(11) | | 2.351(15) | 2.9079(15) | | | 180 |
| *$NdSrScO_4$* | | | | | | | | | |
| 25 | 2.0353(18) | 2.186(12) | 2.783(12) | 2.599(10) | 2.419(15) | 2.8904(23) | 2.262(12) | 3.378(15) | 167.3(9) |
| 50 | 2.0428(21) | 2.201(13) | 2.796(13) | 2.602(11) | 2.462(17) | 2.8994(24) | 2.254(24) | 3.360(17) | 167.0(10) |
| 100 | 2.0427(20) | 2.180(13) | 2.801(13) | 2.603(10) | 2.452(16) | 2.8944(23) | 2.276(13) | 3.373(16) | 166.7(10) |
| 200 | 2.0491(20) | 2.174(13) | 2.832(11) | 2.591(9) | 2.445(15) | 2.8939(21) | 2.296(13) | 3.384(15) | 164.7(8) |
| 300 | 2.0426(19) | 2.152(13) | 2.798(13) | 2.628(11) | 2.453(15) | 2.8935(21) | 2.322(13) | 3.370(15) | 168.5(10) |
| 400 | 2.0405(17) | 2.161(13) | 2.778(15) | 2.652(13) | 2.460(15) | 2.8962(21) | 2.323(13) | 3.367(15) | 170.5(12) |
| 500 | 2.0400(17) | 2.184(13) | 2.767(17) | 2.672(15) | 2.457(16) | 2.9013(23) | 2.307(14) | 3.377(16) | 171.9(14) |
| 600 | 2.0412(20) | 2.173(15) | 2.779(19) | 2.670(17) | 2.447(17) | 2.9031(25) | 2.326(15) | 3.383(17) | 171.1(14) |
| 700 | 2.0391(16) | 2.181(14) | 2.750(2) | 2.705(21) | 2.483(18) | 2.9046(25) | 2.314(15) | 3.348(17) | 174.7(19) |
| 800 | 2.0387(12) | 2.183(16) | 2.727(32) | 2.736(30) | 2.533(22) | 2.9037(26) | 2.303(16) | 3.302(21) | 177.1(27) |
| 900 | 2.0392(4) | 2.177(16) | 2.711(29) | 2.763(28) | 2.550(24) | 2.9033(27) | 2.310(17) | 3.283(23) | 179.0(24) |
| 1000 | 2.0430(22) | 2.195(16) | 2.646(28) | 2.842(29) | 2.537(23) | 2.9109(30) | 2.305(17) | 3.297(22) | 174.3(25) |
| *$SmSrScO_4$* | | | | | | | | | |
| 25 | 2.0449(23) | 2.078(17) | 2.864(11) | 2.573(9) | 2.278(14) | 2.8848(23) | 2.412(17) | 3.479(14) | 162.8(9) |
| 50 | 2.0424(21) | 2.061(16) | 2.847(11) | 2.585(9) | 2.297(14) | 2.8796(21) | 2.420(16) | 3.459(14) | 163.8(8) |
| 100 | 2.0461(21) | 2.069(15) | 2.865(10) | 2.573(8) | 2.294(13) | 2.8813(21) | 2.415(15) | 3.464(13) | 162.6(8) |
| 200 | 2.0439(21) | 2.052(15) | 2.844(11) | 2.587(9) | 2.333(14) | 2.8789(20) | 2.423(15) | 3.435(14) | 164.2(8) |
| 300 | 2.0457(21) | 2.041(15) | 2.844(11) | 2.592(9) | 2.341(14) | 2.8786(19) | 2.436(16) | 3.430(14) | 164.2(9) |
| 400 | 2.0459(21) | 2.033(15) | 2.842(11) | 2.602(9) | 2.348(14) | 2.8797(19) | 2.446(15) | 3.428(14) | 164.8(9) |
| 500 | 2.0483(21) | 2.028(15) | 2.850(11) | 2.604(9) | 2.356(14) | 2.8808(18) | 2.454(16) | 3.421(14) | 164.5(9) |
| 600 | 2.0503(22) | 2.028(15) | 2.860(12) | 2.601(10) | 2.358(14) | 2.8846(19) | 2.461(16) | 3.420(140 | 164.3(9) |
| 700 | 2.0531(24) | 2.029(16) | 2.874(12) | 2.597(10) | 2.403(16) | 2.8837(19) | 2.450(16) | 3.378(16) | 163.7(9) |
| 800 | 2.0533(25) | 2.032(16) | 2.874(14) | 2.605(11) | 2.421(16) | 2.8856(20) | 2.447(16) | 3.363(16) | 164.3(10) |
| 900 | 2.0530(25) | 2.042(16) | 2.874(14) | 2.614(12) | 2.420(16) | 2.8895(20) | 2.445(16) | 3.366(16) | 164.9(11) |
| 1000 | 2.0565(27) | 2.049(17) | 2.896(15) | 2.606(12) | 2.435(17) | 2.8936(22) | 2.441(17) | 3.353(17) | 164.2(11) |

Estimated standard deviations given in parentheses.

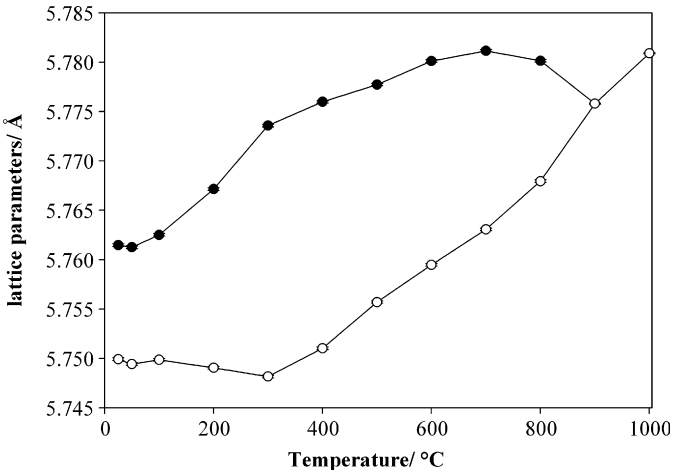


Fig. 3. $a$ and $b$ lattice parameters as a function of temperature for $LaSrScO_4$; ● ($a$ parameter), ○ ($b$ parameter).

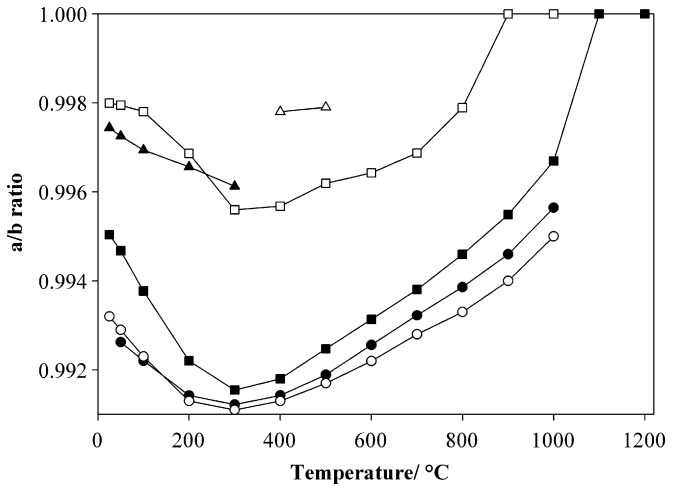


Fig. 4. Temperature dependence of the $a/b$ lattice parameter ratio for $Ln$SrScO$_4$; ▯ (LaSrScO$_4$), ▲ (CeSrScO$_4$), △ (part oxidized CeSrScO$_4$ sample), ■ (PrSrScO$_4$), ● (NdSrScO$_4$), ○ (SmSrScO$_4$).

temperature is to markedly lengthen one of these contacts (from the $A$ site to one of the apical oxygen atoms of the adjacent $BO_4$ layer) while shortening, on average, the remainder producing an, effectively, 8 coordinate site, see Fig. 6. In general, the level of tilting and the tendency of the $Ln$/Sr–O coordination to move towards 8-fold increases as the lanthanide cation size decreases. This behavior mirrors that found in many lanthanide compounds with a tendency to move to lower coordination numbers, but with shorter contacts, as the size of the lanthanide ion decreases across the series La to Lu.

The variable temperature data, summarized in Table 3 and Fig. 4, show that for all compounds $Ln$SrScO$_4$ ($Ln$ = La–Sm) the cell orthorhombicity increases on heating to ~300 °C before decreasing. Extrapolation of the data from $Ln$ = Nd and Sm indicate that a similar phase transition would occur for these materials but only at temperatures close to those at which they were synthesized. This behavior is also reflected in the tilting of the ScO$_6$

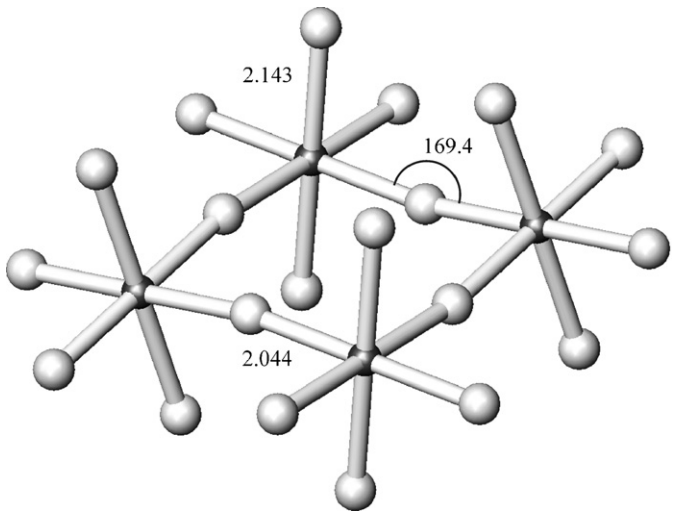


Fig. 5. Coordination environment about $Sc^{3+}$ in $LaSrScO_4$ at room temperature. Axial and equatorial Sc–O bond distances are labeled as is the Sc–O–Sc bond angle.

octahedra as measured by the extracted Sc–O–Sc bond angle which, for all compounds, remains fairly constant or decreases slightly between room temperature and 300 °C before increasing above this temperature; for the compounds with the larger lanthanides, $Ln$ = La and Pr this angle reaches 180 °C and the materials become tetragonal. Note that the trends in this extracted bond angle are less well defined due to significant errors in the extracted O(1) positional parameters; furthermore, the effect of imperfect modeling of the increased thermal motion of this atom at higher temperatures can also influence the extracted bond angle. The origin of this behavior presumably derives from the competing factors associated with the thermal expansion of different structural elements of the materials. Between room temperature and 300 °C this thermal expansion seems to be accommodated in a maintained or an increased tilting of the octahedra (equivalent to a maintained or decreased Sc–O–Sc angle) which allows lengthening of the average Sc–O distances through the general increases in the lattice parameters. Consideration of the $Ln$/Sr environment, Table 4, shows that in general the shorter $Ln$–O interactions also increase in length on heating while the longer $Ln$–O distances actually decrease in length as the overall $Ln$–O coordination geometry becomes more regular. This behavior is most marked above 300 °C as the phases are driven back towards tetragonal symmetry.

## 4. Discussion

In order to investigate the factors that lead to a choice of structure, and drive distortions in oxides adopting the $K_2NiF_4$ structure type away from an $I4/mmm$ description, a further analysis of structural data, using that obtained here and from literature sources, was undertaken. Tolerance factors, $t$, which use the relative sizes of the $A$ and $B$ cation types, can provide a reasonable indication of

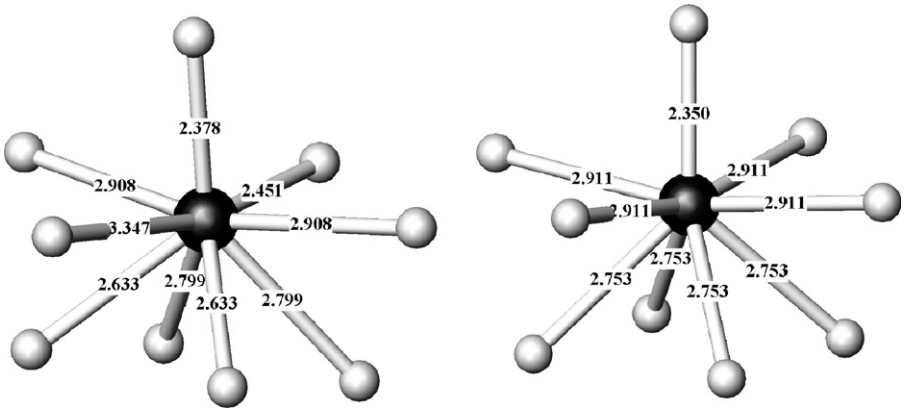


Fig. 6. Coordination environment about $La^{3+}$ in $LaSrScO_4$ at room temperature (left) and at 1000 °C (right). *Ln*/Sr-O bond distances are labeled. Figures are oriented with the equivalent short apical contact vertically in both diagrams.

whether a material with the $K_2NiF_4$ structure-type may have a tendency to distort or not. However, it should be noted that the value of $t$ at which a material chooses to adopt a specific structure type rather than another may depend on additional factors such as spin state, anion type ($O^{2-}$, $F^-$, $Cl^-$ and $N^{3-}$ are all known in $K_2NiF_4$-type structures) and polarization effects.

Before turning to such detailed tolerance factor considerations and calculations it is worth considering how the regular tetragonal $A_2BO_4$ structure can react to changes in the relative sizes of $A$ and $B$. When $A$ is relatively large in comparison with $B$ the network of octahedra is under tension but any tilting of the corner sharing $BO_6$ units would, presumably unfavorably, result in reduction of some $A$–O distances. In this circumstance the system could instead lengthen all the $A$–O interactions by increasing the interlayer separation but maintaining the regular arrangement of $BO_6$ units along the $c$ direction. When $B$ is relatively large in comparison with $A$, the network of octahedra is under compression and this generally leads to a buckling at the shared oxygen apices along the $B$–O–$B$ directions, which can be accommodated by cooperative rotations of the octahedra. This acts to shorten some $A$–O distances while lengthening others producing a more-compact coordination geometry for the relatively smaller $A$-type cation.

The three situations, matched $A$ and $B$, relatively large $A$, and relatively large $B$ can be discussed more quantitatively in terms of the tolerance ratio $t = (r_A + r_O)/\sqrt{2}(r_B + r_O)$. Note that this expression represents the fit between $A$ type cation and one perovskite plane—to which it is formally 8 coordinated—but does not allow for the additional, often very short contact, with the oxygen in the adjacent perovskite layer. Thus when $t = 1$ this would represent a match between $A$, $B$ and O for just one $A$ to perovskite layer interaction rather than the complete $K_2NiF_4$ structure.

A scatter-plot of $K_2NiF_4$ structure-type oxide phases as a function of $A$ cation and $B$ cation sizes using Shannon [17] ionic radii is shown in Fig. 7 and covers systems where $A$ = Ba, Sr, Ca, *Ln* and mixtures thereof and $B = Co^{3+}$, $Sc^{3+}$, $Ni^{3+}$, $Al^{3+}$, $Ga^{3+}$, $V^{3+}$, $Cr^{3+}$, $Fe^{3+}$, $In^{3+}$, $Cu^{3+}$, $Co^{2+}$, $Ni^{2+}$ and $Cu^{2+}$. Lines are plotted on this graph that

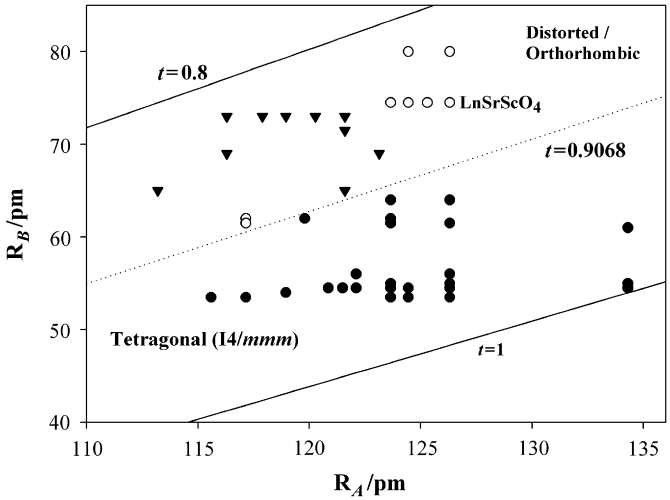


Fig. 7. $A$ cationic radii against $B$ cationic radii for compounds adopting the $A_2BO_4$ structure type: ● (tetragonal $A_2BO_4$), ○ (distorted $A_2BO_4$ ($B^{3+}$)), ▼ (distorted $A_2BO_4$ ($B^{2+}$)).

represent $t = 1$, $t = 0.906$ and $t = 0.8$. It should be noted that no oxide exists with $t > 1$ which would represent a very large $A$ relative to $B$; such a system would require the largest $A$-type cations found in this structure type, i.e. $Ba^{2+}$ in combination with the smallest $B$-type, e.g. $Al^{3+}$ or $Co^{3+}$, for example $LaBaAlO_4$ [18] with $t = 1.002$. In fact $LaBaAlO_4$ adopts a structure with the space group $P2_12_12_1$ containing discrete $AlO_4$ tetrahedra and $Ba_2TiO_4$ [19] ($t = 1.012$) adopts a structure in the space group $P2_1/c$ also with tetrahedral $B$ coordination, $TiO_4^{4-}$. This may indicate that the $K_2NiF_4$ structure cannot accommodate in oxides the coordination preferences of both cations for $t > 1$ (using the Shannon set of ionic radius values). These large values of $t$ require very small $B$-type cations which can also adopt tetrahedral coordination to oxygen; with discrete tetrahedra, such as $AlO_4$ and $TiO_4$, oxygen can then coordinate multiply to the large $A$-type cations. This generates higher coordination numbers for these species, typically 9–12, and other structures become thermodynamically more stable.

For values of $t$ above ~0.9 all compounds adopt the perfect ($I4/mmm$) $A_2BO_4$ structure-type; those below this value are distorted. For example tetragonal ($I4/mmm$) $LaBaCoO_4$ (low spin $Co^{3+}$) ($r_A = 134.3$ pm, $r_B = 54.5$ pm and $t = 0.9972$) is below the threshold and orthorhombic ($Abma$) $La_2CoO_4$ ($r_A = 121.6$, $r_B = 73$ pm and $t = 0.8684$) is above the threshold. The best value delineating the separation between tetragonal and distorted structure type is equivalent to $t = 0.907$ with materials having values lower than this adopting non-$I4/mmm$ descriptions. Clearly for a particular $B$-type cation size, and thus size of $BO_6$ octahedron, there is a minimum $A$ type cation size that can occupy the semi-regular 9-coordinated position; for values smaller than this the $BO_6$ octahedra tend to tilt, rotate or distort so as to modify the coordination of oxygen to the $A$-type cation. Generally these lower symmetry structures, described in spaces groups such as $Abma$ and $Fmmm$, produce a lower number of shorter coordination interactions for the $A$ type cation. $LaSrScO_4$ lies, in this diagram, above the $t = 0.9068$ line with $t = 0.878$ consistent with the experimental observation of a tilting of the $ScO_6$ octahedra.

It also becomes possible to rationalize, to some extent, the high temperature structural behavior of these materials. The greater thermal vibration that occurs with increased temperature allows the tetragonal $K_2NiF_4$ structure to accommodate more readily any mismatch between ion sizes, so effectively the $t$ line separating the two regions moves to lower values. Materials with $t$-values close to the line would be expected to transform to the regular tetragonal structure more readily at higher temperatures than those further away—though such arguments would be tempered by kinetic considerations. This behavior is observed in this work with the two phases with the largest $t$-values, $LaSrScO_4$ and $PrSrScO_4$, transforming to the tetragonal phases on heating to around 900 °C.

It is also possible to use Fig. 7 to predict the stability and structure type of other $A_2BO_4$ phases and, in particular, select the possible lanthanide ionic radii needed to match a specific $B$ cation in a general $Ln$Sr$B$O$_4$ system. Thus for phases of the composition $Ln$SrCoO$_4$ with a smaller $B$ cation radius than used in this work ($r_B$ ($B = Co^{3+}$) = 54.5 pm; $r_B$ ($B = Sc^{3+}$) = 73 pm) it should be possible to synthesize phases with the $K_2NiF_4$ structure for smaller A cations. Thus lanthanides as small as $Gd^{3+}$ ($r_A = 1.24$ Å) should fit into a $K_2NiF_4$-type structure with $Co^{3+}$ yielding $GdSrCoO_4$. This should be compared with the $Ln$SrScO$_4$ system studied here where the smallest lanthanide that can be accommodated by the structure type is $Sm^{3+}$. Attempts to synthesize pure $Ln$BaScO$_4$ phases were also unsuccessful leading to mixtures containing $Ln_2BaSc_2O_7$; with barium replacing strontium the $t$-value increases and a regular $I4/mmm$ structure type might be expected. However, the greater disparity in $La^{3+}$ and $Ba^{2+}$ ionic radii seems to start to favor the formation of the Ruddlesden–Popper 327 structure type where one $A$-type cation, presumably the larger barium, can occupy a site with 12-fold coordination to oxygen.

## 5. Conclusions

An X-ray diffraction study has been performed on the series of compounds $Ln$SrScO$_4$ ($Ln$ = La, Ce, Pr, Nd and Sm) over the temperature range 25–1200 °C. The room temperature structural description of $LaSrScO_4$ has been investigated in various space groups accommodating different $ScO_6$ octahedral tilts as proposed by Hatch et al. [11]. The orthorhombic $Abma$ space group was the most plausible, producing the best final profile fit parameters in terms of the number of refinable parameters. Rietveld refinement of the structures for the $Ln$SrScO$_4$ ($Ln$ = Ce, Pr, Nd and Sm) phases described in $Abma$, using their room temperature PXD data, confirmed this space group description for these materials. Variable temperature PXD studies of all phases $Ln$SrScO$_4$ show that the level of distortion within these compounds increases in the temperature range 25–300 °C and decreases in the temperature range 400–1200 °C. $LaSrScO_4$ and $PrSrScO_4$ revert to the tetragonal $I4/mmm$ space group at 900 and 1000 °C, respectively. A general structural model based on tolerance factors has been developed for the family of materials $A_2BO_4$ with various $A$ and $B$ cation sizes. Based on this study and calculations of tolerance factors, the $Ln$SrScO$_4$ systems are expected to be distorted from the ideal $K_2NiF_4$ structure and become less distorted on heating, consistent with the experimental data.

## Acknowledgment

We thank Dr. Bob Hughes for help with the PXD data collection and useful discussions.

## References

[1] D. Balz, K. Plieth, Z. Elektrochem. 59 (1955) 545.
[2] I. Kozo, Physica C 185–189 (Part 4) (1991) 2509.
[3] J.B. Boyce, F. Bridges, T. Claeson, T.H. Geballe, C.W. Chu, Phys. Rev. B. 35 (1987) 7203.
[4] K.D. Nelson, Z.Q. Mao, Y. Maeno, Y. Liu, Science 306 (2004) 5699.
[5] D.I. Woodward, I.M. Reaney, Acta Crystallogr. B 61 (2005) 387.
[6] P.M. Woodward, Acta Crystallogr. B 53 (1997) 44.
[7] C.J. Howard, H.T. Stokes, Acta Crystallogr. B 54 (1998) 782.
[8] H. Shaked, J.D. Jorgensen, J. Solid State Chem. 154 (2000) 361.
[9] P. Ganguly, C.N.R. Rao, J. Solid State Chem. 53 (1984) 193.
[10] U. Lehmann, H. Mueller-Buschbaum, Z. Anorg. Allg. Chem. 470 (1980) 59.
[11] D.M. Hatch, H.T. Stokes, Phys. Rev. B 39 (1989) 9282.
[12] S. Kato, M. Ogasawara, M. Sugai, S. Nakata, Solid State Ion. 149 (2002) 53.
[13] I.-S. Kim, H. Kawaji, M. Itoh, T. Nakamura, Mater. Res. Bull. 27 (1992) 1193.
[14] H.M. Rietveld, Acta Crystallogr. 22 (1967) 151.
[15] H.M. Rietveld, J. Appl. Crystallogr. 2 (1969) 65.
[16] A.C. Larson, R.B. Von Dreele, Generalised structure analysis system, MS-H805, Los Alamos, NM, 1990.
[17] R.D. Shannon, Acta Crystallogr. A 32 (1976) 751.
[18] J.A. Bland, Acta Crystallogr. 14 (1961) 875.
[19] L.M. Kovba, L.N. Lykova, E.V. Antipov, Koordinats. Khim. 11 (1985) 1574.